

Mechanical properties of Nucleic Acids and the non-local Twistable Wormlike Chain model

Midas Segers,¹ Aderik Voorspoels,¹ Takahiro Sakaue,² and Enrico Carlon^{1, a)}

¹⁾*Soft Matter and Biophysics Unit, KU Leuven, Celestijnenlaan 200D, 3001 Leuven, Belgium*

²⁾*Department of Physical Sciences, Aoyama Gakuin University, 5-10-1 Fuchinobe, Chuo-ku, Sagami-hara, 252-5258, Kanagawa, Japan*

(Dated: August 12, 2022)

Mechanical properties of nucleic acids play an important role in many biological processes which often involve physical deformations of these molecules. At sufficiently long length scales (say above $\sim 20 - 30$ base pairs) the mechanics of DNA and RNA double helices is described by a homogeneous Twistable Wormlike Chain (TWLC), a semiflexible polymer model characterized by twist and bending stiffnesses. At shorter scales this model breaks down for two reasons: the elastic properties become sequence-dependent and the mechanical deformations at distal sites gets coupled. We discuss in this paper the origin of the latter effect using the framework of a non-local Twistable Wormlike Chain (nTWLC). We show, by comparing all-atom simulations data for DNA and RNA double helices, that the non-local couplings are of very similar nature in these two molecules: couplings between distal sites are strong for tilt and twist degrees of freedom and weak for roll. We introduce and analyze a simple double-stranded polymer model which clarifies the origin of this universal distal couplings behavior. In this model, referred to as the ladder model, a nTWLC description emerges from the coarsening of local (atomic) degrees of freedom into angular variables which describe the twist and bending of the molecule. Differently from its local counterpart, the nTWLC is characterized by a length-scale-dependent elasticity. Our analysis predicts that nucleic acids are mechanically softer at the scale of a few base pairs and are asymptotically stiffer at longer length scales, a behavior which matches experimental data.

I. INTRODUCTION

Mechanical properties of nucleic acids are of high relevance in several biological processes (see e.g. Refs. 1–3 for recent reviews) as these molecules are often deformed by the action of ligands or by thermal fluctuations. A large number of studies has provided a good deal of understanding of nucleic acids mechanics, in particular via computer simulations of all-atom^{4–8} or of coarse-grained type^{9–12}. While DNA is most commonly found in a double helical form, RNA is usually a single stranded molecule, but it can also form double helices in cells or viruses. Due to the different chemical nature of their constituent strands (deoxyribose vs. ribose) DNA and RNA form helices with different geometries, known as B and A-forms in the literature, see Fig. 1(a,b). For a recent review of the differences in the mechanics of DNA and RNA see Ref. 3. In this paper we are particularly interested in characterizing non-local couplings which involve non-consecutive base pairs^{5,13–16} (Fig. 1(a)). The aim of this paper is to highlight the similarities and differences between non-local interactions in DNA and RNA and introduce a simple model which provides some quantitative understanding on the general properties of non-local couplings of elastic double-stranded molecules.

At the microscopic scale any conformation of a DNA or RNA double helix can always be given by the Cartesian coordinates of all the atoms. Such detailed description is however not very informative when one analyzes deformations involving several base pairs. For that purpose it is more convenient to use a set of coarse-grained coordinates describing for example bending or twist angles. It is via these coordinates that one

can define, for instance, bending and twist persistence lengths. The number of coarse-grained coordinates used depends on the degree of accuracy one wishes to achieve to describe local deformations. In the rigid base-pair model, base-pairs are modeled as rigid bodies¹⁷. The six variables tilt, roll, twist, shift, slide and rise describe the rotations and displacements of consecutive base pairs. Tilt and roll describe the bending along the two possible bending directions of the helix. The twist describes the rotation along an axis perpendicular to the plane formed by a base pair. Shift, slide and rise describe the displacements of two consecutive base pairs along the three

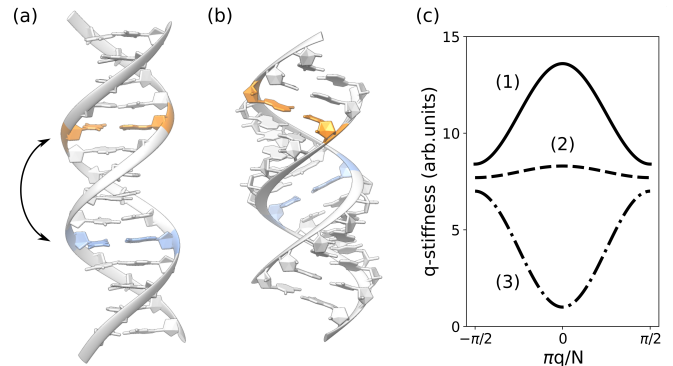


Figure 1. Molecular structures of (a) DNA and (b) RNA double helices. We focus here on the analysis of couplings between distal sites along the helices, as those indicated in colors in (a) and (b). Such interactions are characterized through the determination of momentum space stiffnesses¹³. The plot (c) illustrates possible behaviors of q -stiffnesses, with $q = 0$ corresponding to the long wavelength limit: (1) strong non-locality with stiffening at long distances (maximum at $q = 0$), (2) very weak non-locality and (3) strong non-locality with softening at long distances (minimum at $q = 0$).

^{a)}Electronic mail: enrico.carlon@kuleuven.be

axes. The even more detailed rigid base model includes six additional intra-basepair coordinates¹⁸.

We will show here how, by passing from an atomistic description to a coarser one using angular coordinates (tilt, roll, twist), one naturally introduces non-local couplings in the system. In Sec. II we introduce the general formalism of the non-local Twistable Wormlike Chain (nlTWLC) which is our reference framework to describe coupling between distal sites in a homogeneous semiflexible twistable polymer. This model uses tilt, roll and twist as angular coordinates and neglects translational degrees of freedom. We highlight the differences with the local TWLC and introduce the stiffness matrix in momentum space¹³, which provides a very convenient formalism to discuss distal couplings. In Sec. III we analyze all-atom simulations data describing elasticity of double stranded RNA and compare with earlier DNA data¹³, within the nlTWLC framework. DNA and RNA data show strong similarities which motivated us to look for a simple model that captures the essential universal features of non-locality for both molecules. This is the ladder model introduced in Sec. IV. This model is sufficiently simple so that several quantities can be estimated analytically and shows how non-distal coupling emerge from the coarsening of “atomistic” degrees of freedom. The ladder model naturally explains why couplings between distal sites are weak for roll and strong for tilt. It also indicates that the twist-twist coupling between distal sites may have a genuine non-local origin. Sec. V concludes the paper by highlighting the experimental relevance of our findings.

II. THE NLTWLC AND STIFFNESSES IN FOURIER SPACE

We consider here a description based on the parameters tilt (τ), roll (ρ) and twist (Ω), using a rigid base pair model which neglects translational stretching degrees of freedom. To describe the deformations of the molecule we introduce the three dimensional vector Δ_n , with $n = 0, 1, \dots, N-1$ labeling the sites along the sequence, defined as

$$\Delta_n \equiv (\tau_n - \langle \tau_n \rangle, \rho_n - \langle \rho_n \rangle, \Omega_n - \langle \Omega_n \rangle)^\top \quad (1)$$

with $\langle \cdot \rangle$ denoting equilibrium averages, so that $\langle \Delta_n \rangle = 0$. Small deformations from equilibrium are usually described within the harmonic approximation², with an energy given by

$$\beta E = \frac{a}{2} \sum_n \sum_m \Delta_n^\top M_m^{(n)} \Delta_{n+m}, \quad (2)$$

with $\beta = 1/k_B T$ the inverse temperature, k_B the Boltzmann constant and a the average distance between consecutive base pairs ($a = 0.34$ nm for DNA, whilst $a = 0.37$ nm for dsRNA). It is well-known that local mechanical properties are very strongly influenced by the sequence composition, our aim however is to characterize the properties of non-local couplings averaged over several different sequences. Therefore we neglected sequence inhomogeneities, as such in the rest of the paper we will drop the label (n) from $M_m^{(n)}$. The energy (2)

includes possible couplings between distal sites n and $n+m$, which are encoded in the 3×3 matrix M_m . Setting to zero all matrices $M_m = 0$ for $m \geq 1$, corresponds to considering a local model. In this limit Eq. (2) describes the usual discrete Twistable Wormlike Chain (TWLC). We refer to the model given by (2) with generic distal couplings, as the non-local Twistable Wormlike Chain (nlTWLC). Several all-atom⁴ and coarse-grained simulations¹¹ indicated that in DNA variables on distal sites are correlated, which implies a coupling between them. In previous papers^{13,14} we have investigated non-local couplings in DNA, which we briefly review (Sec. II), before analyzing these interactions in RNA (Sec. III) and discussing a simple model of non-local elasticity (Sec. IV).

A full account of the elastic behavior of a polymer model with non-local interactions has been presented in Ref. 13. Here we give a brief summary of the main results. Non-local couplings are more conveniently described in a momentum-space representation via discrete Fourier transforms of the deformation parameters¹³

$$\tilde{\Delta}_q = \sum_{n=0}^{N-1} \Delta_n e^{-2\pi i q n / N} \quad (3)$$

where $q = -(N-1)/2, -(N-3)/2, \dots, (N-3)/2, (N-1)/2$ (for N odd). As the vector Δ_n contains real numbers, one finds by complex conjugation $\tilde{\Delta}_q^* = \tilde{\Delta}_{-q}$. The nlTWLC (2) in q -space then takes the form

$$\beta E = \frac{a}{2N} \sum_q \tilde{\Delta}_q^\dagger \tilde{M}_q \tilde{\Delta}_q, \quad (4)$$

where the matrices \tilde{M}_q and M_n are related to one another via Fourier transform¹³

$$\tilde{M}_q = \sum_m M_m e^{-2\pi i q m / N} \quad (5)$$

Formally, the step from (2) to (4) requires a system with periodic boundary conditions, which ensure translational invariance. However, the difference between a linear or circular molecule at small deformations is only linked to boundary terms, which do not influence the large N bulk behavior.

Note that in the local model limit (TWLC), corresponding to $M_m = 0$ for $m \geq 1$, the q -space stiffness matrix \tilde{M}_q becomes q -independent. A weak dependence indicates that the stiffness is predominantly determined by local interactions. Conversely, a strong q -dependence reflects strong non-local effects. Non-local couplings give rise to length-scale-dependent elasticity¹³, i.e. the molecule can become either stiffer or softer when its elastic behavior is probed at longer length scales. A maximum in the q -stiffness at $q = 0$ indicates then a stiffening at increasing lengths, as the $q \rightarrow 0$ limit corresponds to the asymptotic long length scale limit $N \rightarrow \infty$ in real space. Fig. 1(c) shows examples of q -space stiffnesses for molecules which are stiffer (1) or softer (3) at increasing lengths.

III. NON-LOCAL COUPLINGS: DNA VS. RNA

In order to assess the presence of possible off-site couplings in RNA duplexes, all-atom MD simulations were performed for several 20-mer sequences (for simulation details see Appendix A). Tilt, roll and twist were extracted from all-atom data using the Curves+ software¹⁹. The vectors $\tilde{\Delta}_q$ were obtained from the discrete Fourier transform (3) and the q -stiffness matrix was calculated from the inversion of the covariance matrix¹³

$$\langle \tilde{\Delta}_q \tilde{\Delta}_q^\dagger \rangle = \frac{N}{a} \tilde{M}_q^{-1} \quad (6)$$

The stiffness matrix in q -space takes the form

$$\tilde{M}_q = \begin{pmatrix} \tilde{A}_q^t & \tilde{D}_q & \tilde{B}_q \\ \tilde{D}_{-q}^* & \tilde{A}_q^r & \tilde{G}_q \\ \tilde{B}_{-q}^* & \tilde{G}_{-q}^* & \tilde{C}_q \end{pmatrix} \quad (7)$$

where the (real) diagonal elements \tilde{A}_q^t , \tilde{A}_q^r and \tilde{C}_q are the tilt, roll and twist stiffness. The matrix \tilde{M}_q is hermitian hence the transposed off-diagonal elements are related by complex conjugation: $\tilde{D}_q^* = \tilde{D}_{-q}$, $\tilde{B}_q^* = \tilde{B}_{-q}$ and $\tilde{G}_q^* = \tilde{G}_{-q}$. Each of these elements have in principle a real and an imaginary part which are respectively symmetric and anti-symmetric in q , as follows from elementary properties of Fourier transforms.

Figure 2(a,b) compares the diagonal terms of DNA (left, Ref. 13) and RNA (right) stiffnesses. Both nucleic acids show a strong q -dependence for the tilt-tilt \tilde{A}_q^t and twist-twist \tilde{C}_q couplings, indicating the presence of significant off-site interactions for these degrees of freedom. Roll deformations, instead, couple predominantly locally for both DNA and RNA, as seen from the weak dependence on q of the roll-roll coupling \tilde{A}_q^r . Off-diagonal stiffnesses for DNA and RNA are shown in Fig. 2(c,d,e,f).

A striking difference between DNA and RNA is that the former has a large twist-roll coupling ($\text{Re} \tilde{G}_q$, Fig. 2(c,d)). Such a coupling was predicted from the general symmetry of the DNA molecule²⁰ and has several consequences on the structure, fluctuations and dynamics of DNA²¹⁻²⁴, but it is much weaker in RNA. To gain some insights about this difference one can consider the structure of DNA and RNA molecules. For this purpose a top view on the plane perpendicular to the base pairs is shown in Fig. 3. Here S_1 and S_2 identify the positions of the sugars of the two backbones, while 1 and 2 label the two axes used in the calculations of the deformation parameters. Rotations about axis 1 from one base pair to the next correspond to tilt deformations, while rotating about axis 2 produces roll deformations. In both DNA and RNA the axis 1 is close to a symmetry axis: a 180° rotation around this axis interchanges the positions of the two strands. On the other hand, the symmetry about axis 2 is broken by the major/minor groove differences in DNA, which is the origin of a twist-roll coupling²⁵. RNA however, from analysis of the molecular structure, seems to have a weaker asymmetry on axis 2 than DNA, which is likely the reason for the weaker

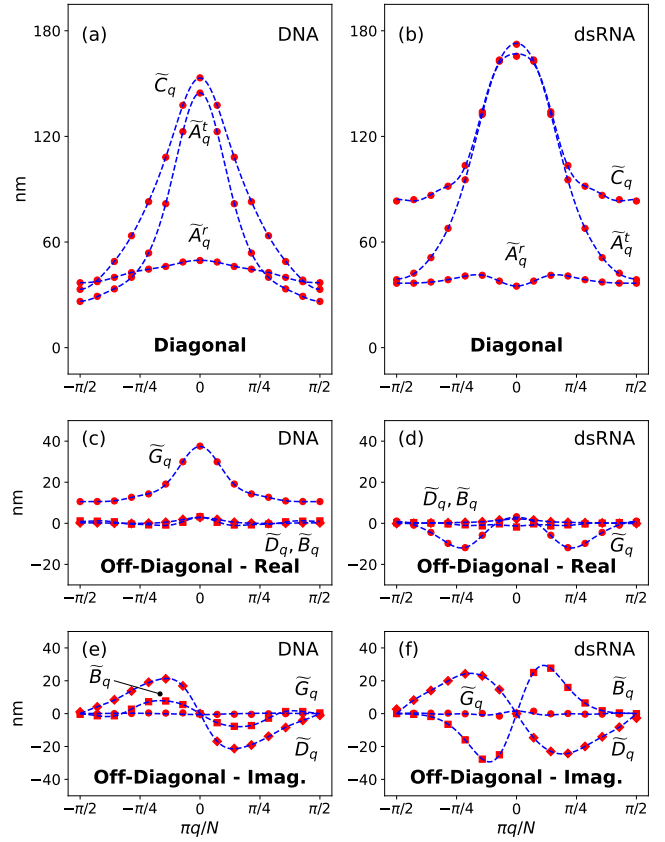


Figure 2. Summary of comparison between elements of momentum space stiffness matrices \tilde{M}_q for DNA (left, Ref. 13) and RNA (right, this work) as obtained from all-atom simulations. The three panels show diagonal elements (a,b), and the real (c,d) and imaginary (e,f) of the off-diagonal coupling terms. The red circles are calculated directly from (6), the blue dashed line represents a fit truncating the Fourier series (5) to a finite number of terms. The fitting parameters are given in Appendix B.

twist-roll coupling. Of course there cannot be exact symmetries due to the chemical differences of the bases. Nonetheless, we note that $\text{Re}(\tilde{G}_q)$, although weak, is larger than other off-diagonal terms in RNA, see Fig. 2(d). Fig. 2(e,f) compares the imaginary parts of the off-diagonal terms, which are anti-symmetric in q . These terms vanish at $q = 0$ and have a small influence on the overall elastic properties of the molecules.

The q -dependence of the stiffness parameters implies length-scale-dependent persistence lengths¹³. A twistable polymer is usually characterized by two persistence lengths associated to bending and twist deformations. We discuss the twist persistence length first. The \tilde{C}_q of Fig. 2(b) is the stiffness for a twist around an axis perpendicular to the base-pair plane, which is tilted with respect to the helical axis, see Fig. 1(b). To describe the experimentally relevant twist around the helical axis, the variable helical twist, $\Omega_n^{(h)}$, as well as the average helical rise, $a^{(h)}$, are used¹⁹. The helical twist correlation function, for a stretch of $m + 1$ base pairs, is defined

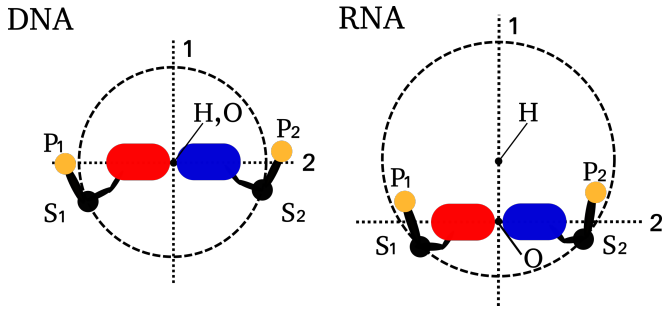


Figure 3. Top view of the molecular structure of DNA and RNA (we draw the RNA structure as planar, in reality the base pair plane is not perpendicular to the helical axis, see Fig. 1(b)). The determination of the tilt, roll and twist parameters is performed by assigning an orthonormal triad associated to each base pair. Triads are centered in “O”, the midpoint of the basepairs, “H” denotes the position of the helical axis. For both molecules the triad is formed by the axis 1 and axis 2 and by a third axis orthogonal to both. In DNA 1 is a symmetry axis, but not 2, which is the origin of the twist-roll coupling²⁵. The molecular structure of RNA suggests a very weak twist-roll coupling as 2 is close to a symmetry axis (see text).

as

$$\left\langle \cos \left(a^{(h)} \sum_{n=0}^{m-1} \Omega_n^{(h)} \right) \right\rangle = e^{-ma^{(h)}/l_T^*(m)} \quad (8)$$

and its decay is governed by the twist correlation length $l_T^*(m)$. Due to couplings between distal sites $l_T^*(m)$ becomes length-scale-dependent. To compute it one can use the relation¹³

$$\frac{1}{l_T^*(m)} = \frac{a^{(h)}}{2\pi m} \int_{-\pi/2}^{\pi/2} \frac{\sin^2 my}{\sin^2 y} \frac{\langle |\tilde{\Omega}_q^{(h)}|^2 \rangle}{N} dy, \quad (9)$$

valid for an infinitely long polymer chain $N \rightarrow \infty$, where $y \equiv \pi q/N$ and where $\tilde{\Omega}_q^{(h)}$ indicates the discrete Fourier transform of $\Omega_n^{(h)}$. For a q -independent stiffness and from the elementary integral

$$\int_{-\pi/2}^{\pi/2} \frac{\sin^2 my}{\sin^2 y} dy = m\pi \quad (10)$$

one finds a length-scale-independent l_T^* , as for the ordinary TWLC. In general, for large m one gets from (9) the following asymptotic expansion¹⁴

$$l_T^*(m) = l_T^*(\infty) \left(1 - \frac{B}{B+m} \right) + \dots \quad (11)$$

with B a coefficient and where the dots indicate exponentially small terms. We obtained the helical twist from simulation data using the Curves+ software¹⁹, given in Fig. 4(a). The blue dashed line is an interpolation of the all-atom data using a truncated Fourier series as explained in Appendix B. These data were used to compute numerically the integral in Eq. (9) and obtained the torsional persistence length $l_T^*(m)$, shown in Fig. 4(b).

To estimate the bending persistence length we used the standard tilt and roll data. Curves+ does not seem to provide

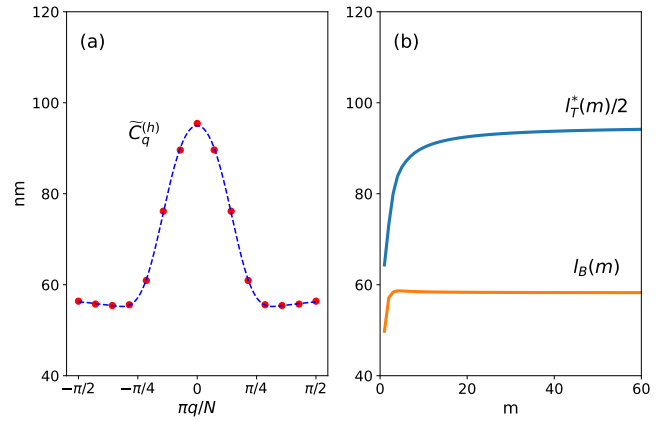


Figure 4. (a) Q-stiffnesses of the helical twist of RNA as obtained from all-atom data. (b) Length-scale-dependence of the twist (blue) and bending (orange) persistence lengths for RNA duplexes. The length-dependence of $l_T^*(m)/2$ is derived from equation (9) using the q -stiffnesses displayed in (a). $l_B(m)$ is acquired using equation (13) along with the attained momentum-space stiffnesses exhibited in Figure 2(b).

these deformations with respect of the helical axis, therefore we will compute a tangent-tangent correlator

$$\langle \hat{t}_n \cdot \hat{t}_{n+m} \rangle = e^{-ma/l_B(m)} \quad (12)$$

with \hat{t}_n perpendicular to the base plane and thus tilted with respect to the helical axis. In the limit of small intrinsic roll and twist, the following expression can be used to estimate the bending persistence length

$$\frac{1}{l_B(m)} = \frac{a}{2\pi m} \int_{-\pi/2}^{\pi/2} \frac{\sin^2 my}{\sin^2 y} \frac{\langle |\tilde{\tau}_q|^2 \rangle + \langle |\tilde{\rho}_q|^2 \rangle}{N} dy \quad (13)$$

which was computed numerically from the interpolated all-atom data (dashed lines of Fig. 2(b,d,f)). The bending persistence length thus obtained is shown in Fig. 4(b). We note that while l_B shows a very modest length-scale-dependence, this dependence is much stronger for l_T^* , in agreement with what has been previously observed for DNA¹³. Both nucleic acids are torsionally softer at short scales and stiffer at longer length scales.

Table I compares the bending and torsional persistence lengths as obtained in this work from q -stiffnesses data, via Eqs. (9) and (13), with other simulation and experimental data from the literature. The bending persistence length reported here is in line with reports from both experimental and simulation studies. Much less has been reported on the twist persistence length, especially from the experimental side. Nonetheless the values calculated here based on momentum space considerations are in agreement with the existing literature.

IV. ORIGIN OF NON-LOCAL ELASTICITY: INSIGHTS FROM SIMPLE MODELS

Having discussed non-local couplings in RNA and underlined the similarities with earlier DNA data¹³, we now inves-

l_B (nm)	$l_T^*/2$ (nm)	Method	Ref.
58 ± 1	94 ± 2	all-atom MD	this work
59 ± 1	100 ± 2	all-atom MD*	this work
59 ± 2	100 ± 2	Magnetic tweezers	[26]
60 ± 3	–	Optical tweezers	[27]
66 ± 1	75 ± 6	all-atom MD	[28]
63.8 ± 0.7	–	Magnetic tweezers/ AFM	[29]
78.9 ± 3.4	108 ± 3	all-atom MD	[30]

Table I. Summary of comparisons of RNA duplex persistence lengths as obtained from the analysis of all-atom data in this paper and experimental and simulation data from existing literature. The error on the values reported in this paper was estimated from the standard deviation of the data across different sequences. We provide two estimates: one is obtained by using the average over all simulated sequences and another (marked with ‘*’) removing three outlier sequences showing a stiffness behavior strongly deviating from the average, see Appendix A. The reported values correspond well to the experiments²⁶. It should however be noted that even though the error is small questions remain regarding the proper definition of l_B when comparing to experiments.

tigate the origin of these couplings using a minimal model of elastic polymer chain with twist and bending degrees of freedom. The model, with an appropriate choice of couplings, can reproduce qualitatively the q -stiffness spectrum which characterizes the elastic behavior of nucleic acids.

A. Ladder Model

We consider an homogeneous mechanical system which consists of a set of point-masses organised into two distinct strands, as illustrated in Fig. 5. We refer to it as the ladder model. Neighbouring masses interact with one another through four distinct interaction types: bonds, backbone rigidity, angular rigidity and stacking, each characterized by a corresponding stiffness. To describe a conformation we use vectors \vec{u}_n and \vec{v}_n which connect neighboring masses along the two strands and vectors \vec{x}_n to describe the orientations of the rungs of the ladder (Fig. 5). We indicate with $\theta_{i,n}$ the angles formed between the backbones and rung vectors, as shown in Fig. 5. The energy of the model is given by

$$\begin{aligned}
\beta E = & \frac{K_s}{2} \sum_n [(|\vec{x}_n| - l_0)^2 + (|\vec{u}_n| - l_0)^2 + (|\vec{v}_n| - l_0)^2] \\
& - K_{wlc} \sum_n (\hat{u}_n \cdot \hat{u}_{n+1} + \hat{v}_n \cdot \hat{v}_{n+1}) \\
& - K_a \sum_n \sum_{i=1}^4 \sin \theta_{i,n} - K_{st} \sum_n \hat{x}_n \cdot \hat{x}_{n+1}
\end{aligned} \quad (14)$$

where $\beta = 1/k_B T$ and where we used $\hat{u}_n \equiv \vec{u}_n/|\vec{u}_n|$, $\hat{v}_n \equiv \vec{v}_n/|\vec{v}_n|$ and $\hat{x}_n \equiv \vec{x}_n/|\vec{x}_n|$ to denote unit vectors. K_s is the spring constant which governs the stretching energy of the bond vectors and l_0 the rest length. Each backbone is modelled as a Worm-Like-Chain (WLC) such that the alignment of subsequent bond vectors i.e. \vec{u}_n, \vec{u}_{n+1} and \vec{v}_n, \vec{v}_{n+1} is energetically favorable. The interaction strength is indicated as K_{wlc} . The model also contains an angular coupling, favoring $\theta_{i,n} = \pi/2$

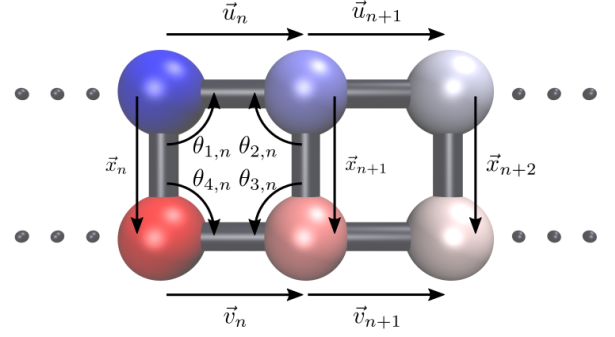


Figure 5. Schematic of the ladder model in its ground-state configuration. Intra- and inter-strand bond vectors are denoted with \vec{u} , \vec{v} and \vec{x} respectively.

angles between adjacent backbone and rung bonds (the angles $\theta_{i,n}$ are defined in Fig. 5). The angular stiffness is governed by the parameter K_a . Additionally the model has a stacking-type of interaction, with stiffness K_{st} , favoring the alignment of consecutive rung vectors \vec{x}_n and \vec{x}_{n+1} .

The lowest energy state of the system consists of a flat ladder with bond vectors of fixed length $|\vec{x}_n| = |\vec{u}_n| = |\vec{v}_n| = l_0$, with the backbone vectors \vec{u}_n, \vec{v}_n all parallel and orthogonal to the rung vectors \vec{x}_n . Thermal excitations distort the ladder inducing bending and twist deformations whose magnitude depends on the values of the stiffness constants K_s, K_{wlc}, K_a and K_{st} . We have set the stiffnesses such that at the level of neighboring base pairs the distortion of angles and bond lengths is weak, e.g.

$$\left| \theta_{i,n} - \frac{\pi}{2} \right| \ll 1, \quad ||\vec{x}_n| - l_0| \ll l_0 \quad (15)$$

1. Elementary excitations

Before considering the elastic behavior of the ladder model and the q -stiffnesses, we analyze three elementary bending deformations which are useful for the following discussion. The calculation gives some indications on the general behavior of the system. These deformations are shown in Fig. 6. The case (a) is referred to as a roll deformation, while (b) and (c) are tilt deformations, in analogy with the nomenclature used for nucleic acids¹⁹. We refer to (a) as a V-bend, to (b) as a C-bend and to (c) as a Z-bend. Now, we will estimate the energy cost associated to the three bends.

The V-bend (a) is a rotation of part of the ladder around a rung. Bonds are not stretched, the inner angles maintain their ground state value $\theta_{i,n} = \pi/2$ and rungs remain parallel. From (14), we obtain the following energy for this deformation

$$\beta \Delta E_V^\phi = 2K_{wlc}(1 - \cos \phi) \quad (16)$$

where ϕ is the rotation angle. This is analogous to a bending deformation in a simple ‘‘local’’ WLC model, the factor 2 accounting for the fact that the two backbones are bent. The C-bend tilt of Fig 6(b) keeps the rungs of the ladder unstretched,

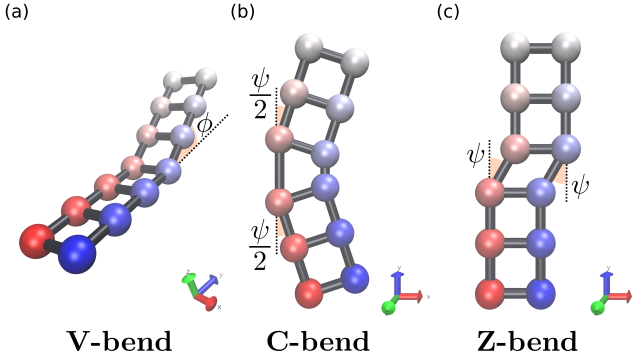


Figure 6. Elementary bending deformations of the ladder model. (a) Example of roll deformation, a bending out of the ladder plane. (b,c) Examples of tilt deformations, which are bendings within the ladder plane. Whereas the bending (a) - here referred to as “V-bend” - is localized to a single ladder rung, (b) and (c) - denoted as “C-bend” and “Z-bend” respectively - consist of the tilting of two consecutive rungs. Whilst the two bending angles in a C-bend are identical, they are opposite in the Z-bend. The excitation energies corresponding to each deformation are given in Eqs. (16), (17) and (18).

but there is some stretching in the backbone bonds. Minimizing this stretching energy we get from (14) the following excitation energy for the C-bend deformation

$$\beta\Delta E_C^\tau = K_S l_0^2 \sin^2 \frac{\Psi}{2} + 4(K_{wlc} + K_a) \left(1 - \cos \frac{\Psi}{2}\right) + K_{st} (1 - \cos \Psi) \quad (17)$$

The C-bend describes a sequence of two bends of an angle $\psi/2$ each. All the four microscopic stiffnesses K_S , K_{wlc} , K_a and K_{st} contribute to this excitation energy. Finally, the Z-bend tilt deformation of type (c) does not involve bond stretching or stacking interaction, as it is only influenced by backbone bending and angle deformation. We find

$$\beta\Delta E_Z^\tau = 4(K_a + K_{wlc})(1 - \cos \psi). \quad (18)$$

Note that for small angles ($|\phi|, |\psi| \ll 1$) the deformation energies (16), (17), (18) are quadratic in ϕ and ψ to lowest order.

Although the above estimates are very simple, they already illustrate some basic features of the model. Roll degrees of freedom are expected to behave as the standard “local” WLC model. As in that case neighboring rolls involving two consecutive angles say ϕ_n and ϕ_{n+1} will be independent: their contribution to the total energy of the molecule is expected to be additive. The situation is very different for tilt. Especially in the case of very large stretching or stacking stiffnesses (large K_S or K_{st}), the system will avoid energetically costly C-bends and favor a large number of Z-bends. Consecutive tilt angles ψ_n and ψ_{n+1} will tend to have opposite signs (they are anti-correlated). This induces an effective coupling between them. As a result of the proliferation of Z-bends the ladder will be soft at short scales and stiffer at long scales. Summarizing, the calculations of these three elementary excitations indicate that the roll stiffness will be very weakly dependent on q , while the tilt stiffness is expected to have a maximum at $q = 0$ (long

wavelength behavior). This is indeed in line with the roll and tilt behavior of DNA and RNA reported in Fig. 2(a,b).

2. Triad definition

In order to calculate stiffness matrices from simulations we need to define bending and twist angles. This is done first by associating local orthonormal triads to each pair of consecutive rungs. This is the procedure usually followed in all-atom¹⁹ as well as in coarse-grained models¹¹. For the ladder model we define a local tangent vector as follows

$$\hat{e}_{3,n} \equiv \frac{\hat{u}_n + \hat{v}_n}{|\hat{u}_n + \hat{v}_n|} \quad (19)$$

In the above the unit vectors \hat{u}_n and \hat{v}_n describe the local orientation of the individual backbones. The second component is defined through the normal of the average plane formed by two subsequent rungs:

$$\vec{n}_n \equiv \frac{\vec{x}_n \times \vec{v}_n}{|\vec{x}_n \times \vec{v}_n|} + \frac{\vec{x}_n \times \vec{u}_n}{|\vec{x}_n \times \vec{u}_n|} \quad (20)$$

Such that:

$$\hat{e}_{1,n} \equiv \frac{\vec{n}_n - (\vec{n}_n \cdot \hat{e}_{3,n})\hat{e}_{3,n}}{|\vec{n}_n - (\vec{n}_n \cdot \hat{e}_{3,n})\hat{e}_{3,n}|} \quad (21)$$

is a unit vector normal to $\hat{e}_{3,n}$. The last component of the triad can be defined from the prior elements through a vector product:

$$\hat{e}_{2,n} \equiv \hat{e}_{3,n} \times \hat{e}_{1,n} \quad (22)$$

By construction $\mathcal{T}_n \equiv \{\hat{e}_{1,n}, \hat{e}_{2,n}, \hat{e}_{3,n}\}$ defines a local orthonormal triad. Consecutive triads \mathcal{T}_n and \mathcal{T}_{n+1} can be mapped onto one another via a rotation characterized by an Euler vector $\vec{\Theta}_n$. The direction of $\vec{\Theta}_n$ defines the rotation axis and its magnitude $|\vec{\Theta}_n|$ is the rotation angle, following the right hand rule. The components of $\vec{\Theta}_n$ in terms of the basis of \mathcal{T}_n define the tilt, roll and twist components

$$\vec{\Theta}_n = l_0 (\tau_n \hat{e}_{1,n} + \rho_n \hat{e}_{2,n} + \Omega_n \hat{e}_{3,n}) \quad (23)$$

We note that τ_n , ρ_n and Ω_n have the dimensions of an inverse length and that $l_0 \tau_n$, $l_0 \rho_n$ and $l_0 \Omega_n$ are the tilt, roll and twist angles expressed in radians. The triad definition is not unique and alternatives are possible. Different triad definitions typically influence the definition of short scale stiffness constants¹¹, but not the long wavelength behavior $q \rightarrow 0$.

3. Stiffnesses from Monte Carlo simulations

We performed Monte Carlo simulations of the ladder model (14). In these simulations a new configuration is generated using a combination of local and global moves which displace masses, or change local bending and twist angles. Configurations are accepted/rejected using the Metropolis algorithm.

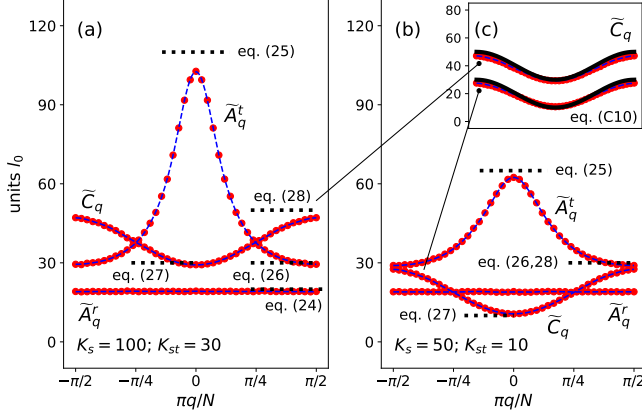


Figure 7. Comparison of momentum space elasticity coefficients for the ladder model with $K_{wlc} = K_a = 10$ and (a) $K_s = 100$, $K_{st} = 30$ (b) $K_s = 50$, $K_{st} = 10$. Both of the simulated ladders consisted of 50 rungs. The dotted lines are the estimates of \tilde{A}_q^r from Eq. (24), and of \tilde{A}_q^t and \tilde{C}_q at $q = 0$ and $q = q_{\max}$ from (25), (26), (27) and (28). The inset (c) compares the q -dependence of the twist stiffness derived for a general twist q -mode (see Appendix C) given by Eq. (C10) (black) with the results obtained from both simulations.

Tilt, roll and twist were calculated from equilibrium sampling using (23). From discrete Fourier transformation we obtained the q -stiffness matrix \tilde{M}_q using (6).

Figure 7 shows a plot of the diagonal elements of \tilde{M}_q for two different sets of parameters. We find virtually no off-diagonal components in the stiffness matrix of the ladder model, so our discussion from now on will be restricted to diagonal terms. We note that the roll q -stiffness \tilde{A}_q^r in Fig. 7 is basically independent on q . This is a consequence of the local and additive nature of roll deformations discussed in the previous section. Since the roll is essentially due to independent V-bends as that in Fig. 6(a), the Fourier transform of Eq. (16), at small angles, gives a q -independent roll stiffness

$$\tilde{A}_q^r = 2K_{wlc} \quad (24)$$

which reproduces well the data of Fig. 7.

The tilt stiffness \tilde{A}_q^t instead exhibits a marked dependence on q , with a maximum at $q = 0$. The comparison between Fig. 7(a) and (b) shows that the q -dependence becomes stronger as the stretching and stacking couplings (K_s and K_{st}) increase. To understand the tilt behavior we estimate the energy associated to the modes $q = 0$ and $q = q_{\max} = (N-1)/2$. Let us consider first a pure $q = 0$ mode, i.e. an excitation of the type $\tilde{\tau}_q = N\alpha\delta_{q,0}$, with $\delta_{m,n}$ the Kronecker delta and α an amplitude, where without loss of generality α can be assumed to be real. Inverse Fourier transforming gives $\tau_n = \alpha$, corresponding to a deformation with constant tilt angle $l_0\alpha$ at every site. This deformation is shown in Fig. 8(a). We can estimate its energy as done for the C-bend deformation (17), assuming that such configuration is obtained as a sequence of symmetric trapezoids as that of Fig. 6(b) in the limit of small

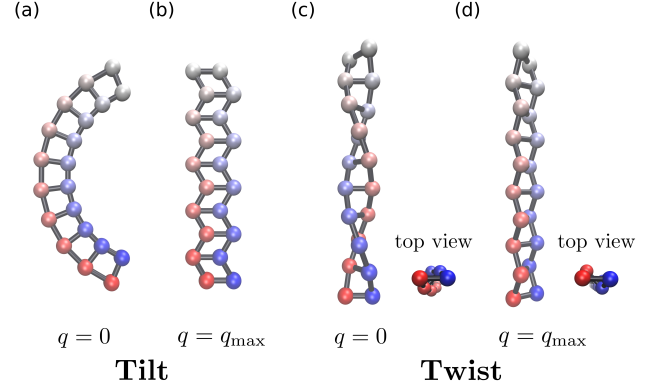


Figure 8. Ladder configurations corresponding to distinct q -modes: $q = 0$ for (a,c) and $q = (N-1)/2$ for (b,d). (a,b) and (c,d) represent pure tilt and twist deformations, respectively. The ladders displayed are small subsystems extracted from infinitely long ladders, such that on the scale of the figure angular modulation for (b,d) are omitted.

angles. From this, we identify the stiffness of this mode

$$\tilde{A}_{q=0}^t = \frac{K_s l_0^2}{2} + 2K_{wlc} + K_a + K_{st} \quad (25)$$

In the following we consider a deformation of the type $\tilde{\tau}_q = \frac{N}{2} [\alpha\delta_{q,q_{\max}} + \alpha\delta_{q,-q_{\max}}]$. The inverse Fourier transform of the q_{\max} -mode reads $\tau_n = (-1)^n \alpha \cos(\frac{\pi n}{N})$, which corresponds to a sequence of angles having alternating signs and a magnitude α which is modulated with $\cos(\frac{\pi n}{N})$.

Figure 8(b) displays a short segment of an infinitely long ladder compliant with the q_{\max} -mode. As $\cos(\frac{\pi n}{N})$ is a weakly varying function for large N , it is rendered constant on the length-scale depicted in the figure. We assume this configuration is obtained by a sequence of Z-bends of Fig. 6(c). We note that if $l_0\alpha$ is the angle between consecutive backbone vectors, the angles within each square are $\theta_{i,n} = \pi/2 \pm l_0\alpha/2$. Following the same calculation as (18) we find the following stiffness for the mode q_{\max}

$$\tilde{A}_{q=q_{\max}}^t = 2K_{wlc} + K_a \quad (26)$$

Equations (25) and (26) approximate well the maximum ($q = 0$) and the minimum ($q = q_{\max}$) of the tilt stiffness, as shown in Fig. 7. The slight overestimation of Eq. (25) may be ascribed to the entropy effect, which is neglected in the above estimation.

There is a striking difference in the behavior of \tilde{C}_q between nucleic acids and ladder model. In DNA and RNA the twist stiffness has a maximum at $q = 0$, indicating that these molecules are torsionally stiffer at long distances, see Fig. 2(a,b) and Fig. 4. The ladder model (14) is torsionally softer at long distances, \tilde{C}_q being minimal in the long wavelength limit $q \rightarrow 0$, see Fig. 7. To understand this behavior we have calculated the twist stiffness for the mode $q = 0$ and $q = q_{\max}$, which are shown in Fig. 8(c) and (d), respectively. As seen for the tilt, the $q = 0$ mode has a constant twist angle, while the $q = q_{\max}$ is formed by a sequence of twist angles

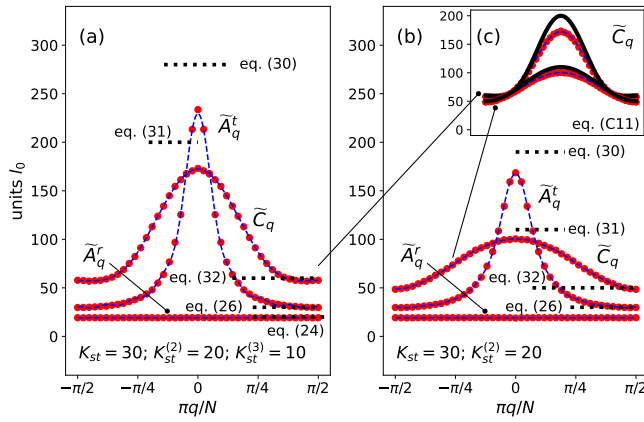


Figure 9. Comparison of momentum space elasticity coefficients of two non-local ladders having a different degree of non-locality. (a) Stacking interactions range between nearest, next-nearest and next-next-nearest neighbors with corresponding magnitudes $K_{st} = 30$, $K_{st}^{(2)} = 20$ and $K_{st}^{(3)} = 10$. (b) Stacking interactions between nearest and next-nearest neighbors with strengths $K_{st} = 30$ and $K_{st}^{(2)} = 20$ respectively. Other microscopic stiffnesses were identical for both ladders: $K_{wlc} = K_a = 10$ and $K_s = 100$. Each of the simulated ladders was comprised of 50 rungs. The dotted lines are the estimates of \tilde{A}_q^r from Eq. (24), and of \tilde{A}_q^t and \tilde{C}_q at $q = 0$ and $q = q_{\max}$ from (30), (26), (31) and (32). The inset (c) shows a comparison of Monte Carlo simulations data for the twist stiffness (red circles) with Eq. (C11) (thick black line).

of magnitude weighed by $\cos\left(\frac{\pi n}{N}\right)$ and alternating signs. We find (for details see Appendix C)

$$\tilde{C}_{q=0} = K_{st} \quad (27)$$

and

$$\tilde{C}_{q=q_{\max}} = 2K_{wlc} + K_{st} \quad (28)$$

The two previous equations are in very good agreement with the data of Fig. 7. Compared to the $q = 0$ case, the ladder backbone is more strongly bent in the mode $q = q_{\max}$, which underlies the observed property $\tilde{C}_{q=0} < \tilde{C}_{q=q_{\max}}$. The backbone bending at $q = 0$ contributes only with higher order anharmonic terms to the energy (see Appendix C), hence the stiffness $\tilde{C}_{q=q_{\max}}$ is independent of the backbone rigidity K_{wlc} . For the twist stiffness, it is possible to generalize the calculations to all q . The estimate is given in Appendix C. A comparison with the simulations is shown in Fig. 7(c).

Having explained the origin of the $q = 0$ minimum of the twist stiffness, one may ask if it is possible to extend the model (14) to have a maximum in \tilde{C}_q at $q = 0$, as seen in nucleic acids data. To achieve this we consider a model where stacking interactions are extended to further neighbors:

$$\beta E^* = \beta E - \sum_n \sum_{l>1} K_{st}^{(l)} \hat{x}_n \cdot \hat{x}_{n+l} \quad (29)$$

where βE is the energy of the model (14). In practice at most two additional couplings $K_{st}^{(2)}$ and $K_{st}^{(3)}$ were considered. A

$K_{st}^{(2)} > 0$ favors alignment of next-neighboring rungs \hat{x}_n and \hat{x}_{n+2} , thereby penalizing the tilt and twist modes $q = 0$. A simple calculation shows that

$$\tilde{A}_{q=0}^t = \frac{K_s l_0^2}{2} + 2K_{wlc} + K_a + K_{st} + \sum_{l>1} l^2 K_{st}^{(l)} \quad (30)$$

and

$$\tilde{C}_{q=0} = K_{st} + \sum_{l>1} l^2 K_{st}^{(l)} \quad (31)$$

For the q_{\max} mode we have instead

$$\tilde{C}_{q=q_{\max}} = 2K_{wlc} + K_{st} + \sum_{l>1} c_l K_{st}^{(l)} \quad (32)$$

with $c_l = 0$ for l even and $c_l = 1$ for l odd. The tilt stiffness at $q = q_{\max}$ (26) does not get affected by the additional stacking terms, as the rungs remain parallel to each other for this deformation. Figure 9(a,b) shows the results of Monte Carlo simulations of the model (29) for two different sets of parameters. Figure 9(c) shows a detail of the comparison of the estimated twist stiffness for all q ((C11), Appendix C). This minimal ladder model reproduces the main features of the q -stiffnesses obtained from all-atom data of Fig. 2. The estimates of the stiffnesses from Eqs. (30) and (31) are in worse agreement with the data when compared with the counterparts (25) and (27) for the original model (14). Again, the analytical estimates neglect entropic contributions which become more relevant when distal interactions are considered. However, for the parameter sets considered the error is of about 15%. Although we have limited our discussion here to a ‘‘flat’’ ladder, very similar stiffnesses as those shown in Fig. 7 and 9 are found in a ladder model with intrinsic twist³¹, which mimicks the double helical structure of nucleic acids.

4. Persistence lengths

Similar to nucleic acids, the elasticity of the ladder model can be characterised by the bending- and twist persistence lengths. Figure 10(a,b) displays the persistence lengths for a local and non-local ladder respectively as derived from two independent methods. The first approach utilizes the attained q -stiffnesses (Fig. 7(a) and 9(b)) from which the twist and bending persistence lengths can be extracted through application of equations (9) (using \tilde{C}_q instead of its helical equivalent) and (13) correspondingly. The obtained results are indicated with the solid lines. The second method consisted of the inversion of the twist and tangent-tangent correlation functions given by formulas (8) and (12). Results acquired in this fashion are represented by the dashed lines. The good agreement between the two approaches brings additional support to the calculations of the RNA bending and torsional persistence lengths, where only the first method could be applied, as sequences analyzed are too short (Table II) to obtain the asymptotic decay of correlation functions.

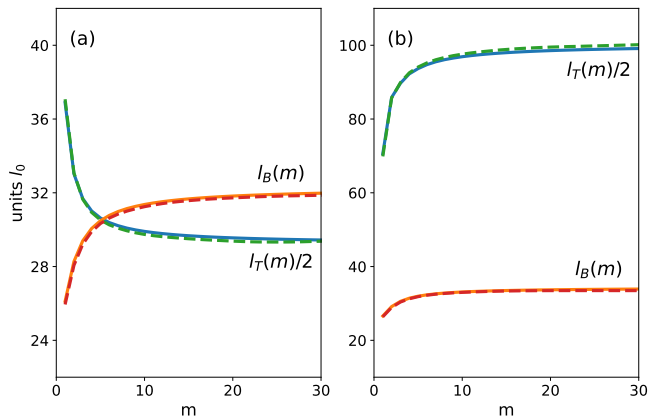


Figure 10. Length-scale-dependent twist- and bending persistence lengths attained using two distinct methods: one based on the obtained q -stiffnesses using equations (9) and (13) (solid lines) and the other using the twist- and tangent-tangent correlation functions defined by (8) and (12) (dashed lines). The two cases correspond to ladders encompassing 50 rungs with stiffnesses (a) $K_s = 100$, $K_{wlc} = 10$, $K_a = 10$ and $K_{st} = 30$ (same as Fig. 7(a)) and (b) $K_s = 100$, $K_{wlc} = 10$, $K_a = 10$, $K_{st} = 30$ and $K_{st}^{(2)} = 20$ (same as Fig. 9(b)). We note that in the case (a) the ladder is torsionally stiffer at short distances and softer at long distances. The opposite is true in the case (b).

V. DISCUSSION

In this paper we have analyzed mechanical interactions of nucleic acids focusing on couplings between distal sites. We have discussed these interactions in the context of the nTWLC using tilt, roll and twist degrees of freedom. Non-locality in real space couplings is most conveniently analyzed in Fourier space: translational invariance, obtained when averaging over different sequence compositions, implies that modes with different q are uncoupled. Using all-atom simulations we have computed the RNA q -stiffnesses and compared with those of DNA, analyzed in a previous publication¹³. Despite their close chemical structure, DNA and RNA form different helices, as illustrated in Fig. 1a. There are some strong qualitative similarities in the mechanical properties of DNA and RNA which can be summarized in three main points: 1) the roll stiffness is weakly dependent on q , 2) tilt and twist stiffnesses are strongly q -dependent and 3) both molecules, in the bending and in the twist behavior, are soft at short length-scales and stiff at long length-scales. One difference between DNA and RNA is that the former has a strong non-diagonal twist-roll coupling, while this is very weak in the latter. Interpolating all-atom q -stiffness data for short molecules (20-mers) using Fourier series we can use analytical expressions derived in Ref. 13 to estimate bending and torsional persistence length for a long RNA molecule. The asymptotic estimates for l_B and l_T are in agreement with literature values (as we have noted, in our analysis, l_B is determined with respect to an axis perpendicular to the base pair plane and not to the helical axis).

One fundamental prediction of the nTWLC is the length-scale-dependent elasticity, meaning that the stiffness of the

molecule is different at different length scales (we note that other polymer models predict such behavior^{32,33}). As observed earlier for DNA¹³, also the RNA appears to be softer at short distances and stiffer at longer distances. This behavior is illustrated in Fig. 4b showing length-dependence expressed in units of base pairs of the bending and torsional persistence lengths for RNA, as obtained from the analysis of all-atom data. These results are qualitatively very similar to those of DNA¹³. The bending persistence length is weakly length-scale-dependent, but there is strong dependence in the torsional response. This implies that one has to be careful to deduce torsional stiffnesses from experiments as the results are expected to depend on the probed distance. Magnetic Tweezers probe the torsional properties of the two ends of ~ 10 kbp molecules²⁶, corresponding to the asymptotic long length-scale behavior. One could also measure the twist stiffness by using local probes, such as by fluorescent labels. From the emission spectrum of a label one can deduce twist fluctuations and thus the twist stiffness³⁴, but this is the torsional stiffness associated to a single base pair, corresponding to $m = 1$ in Fig. 4b. In fact local probe methods provide systematically lower twist stiffnesses for DNA, as opposed to the tweezers data³⁵. In biological systems, double stranded nucleic acids are deformed at different length scales. Cells may exploit the DNA and RNA local flexibility in processes that require the deformation of nucleic acids at short scales. For instance, the interaction between DNA and DNA-bending proteins may be facilitated by local DNA flexibility.

We have shown that a minimal “ladder” model of double stranded polymer reproduces several features of q -stiffnesses observed in RNA and DNA all atom simulations. Although microscopic interactions in the ladder are almost all of local nature (except for stacking), the analysis shows that non-locality emerges naturally when coarse-grained variables as tilt, roll and twist are used. The ladder model explains very naturally the weak dependence on q for the roll and it is sufficiently simple so that several analytical calculations are possible. These calculations link the microscopic parameters which are bond stretching and angular stiffnesses to the coarse-grained stiffnesses for tilt, roll and twist at least for the modes $q = 0$ and $q = q_{\max}$.

All-atom simulations, even when restricted to short sequences, say 20 – 30-mers, require a substantial computational effort. Many simpler coarse-grained models have been devised³⁶ to provide accurate information about DNA mechanics, but bypassing the complexity of a simulation at all-atom scale. Examples are the rigid base-pair model¹⁹, the rigid base model¹⁸ and the more recent multi-modal model⁸, which goes beyond the harmonic approximation. These models use a set of coarse-grained coordinates and sample the DNA conformation of long molecules using Monte Carlo methods. The parametrization is based on a large set of sequence-dependent tetranucleotide stiffnesses. It would be interesting to test how well these coarse-grained model reproduce the sequence dependent q -stiffnesses of Appendix A as these quantities sample simultaneously the short and long scale behavior.

Finally we comment on some issues with the continuous

limit of the nTWLC. Such limit is often used in the TWLC. We discuss here the case of a one component system described by a single variable x_n , but the discussion can be easily generalized to more components such as tilt, roll and twist. In q -space the energy is given by

$$\beta E = \frac{1}{2N} \sum_q \tilde{K}_q |\tilde{x}_q|^2 \quad (33)$$

where the variable \tilde{x}_q is obtained from the discrete Fourier transform of x_n . The continuum long wavelength limit is obtained by approximating the previous expression using an expansion of \tilde{K}_q around $q = 0$. As the energy is symmetric in q the expansion gives:

$$\beta E \approx \int_{-\Lambda}^{\Lambda} \frac{dq}{2N} (\tilde{K}_0 + q^2 \Gamma) |\tilde{x}_q|^2 \quad (34)$$

where we have introduced a short scale momentum cutoff Λ . Let us consider the case $\Gamma > 0$ first. In the calculation of several quantities (as correlation functions), one can safely take the $\Lambda \rightarrow \infty$ limit. Modes with large $|q|$ have high energy and have low statistical weight, that is why many quantities are cutoff independent. Transforming back into real space and using a continuous variable $x(s)$ one gets

$$\beta E = \int_0^L ds \left[\frac{\tilde{K}_0}{2} x^2(s) + \frac{\Gamma}{2} (\partial_s x(s))^2 \right] \quad (35)$$

This is similar to the model of twist dynamics discussed in Ref. 37. However, the situation is quite different for $\Gamma < 0$, which is the relevant case for nucleic acids. All quantities become cutoff dependent because modes such that

$$|q| > q^* = \sqrt{-\tilde{K}_0/\Gamma} \quad (36)$$

have negative energy and are unstable. Therefore the cutoff plays an essential role for $\Gamma < 0$. Generalizing to higher dimension we note that the stiffness matrix \tilde{M}_q may contain imaginary off-diagonal elements which are antisymmetric in q . These can be written as total derivatives and do not contribute to the continuum model limit.

In conclusion, we have shown that length-scale-dependent stiffness is a universal property of double stranded nucleic acids, and that such behavior is also found in a minimal ladder model. The emergence of non-locality is mainly a consequence of coarse-graining for tilt deformations, while the twist behaviour is more complex in origin. Both however are well described by a nTWLC model. We expect that such effects should be relevant for other polymers as well.

ACKNOWLEDGMENTS

Discussions with E. Skoruppa are gratefully acknowledged. T.S was supported by JSPS KAKENHI (grant numbers: JP18H05529, 21H05759)

Color	Sequence	sim. time (ns)
■	AAAACGAGGAUCUUUUCUCG *	10 / 100
■	AGCUGUGCUACCUAUAGCUG	10 / 100
■	GAUCGCAAGUUGAGACCACG	10 / 100
■	GGACACGUCGGGAGGGUUUU	10 / 100
■	GUAACCUUGGCUACGAAUGGC	10 / 100
■	GCAUGCAUGACUAGCAUGCA	10
■	GAUGACGUACUAGCGCAGCA	10
■	UUAGCAUGAUCAUAACGCAA	10
■	GUCCACAAAGUUGAUGCUAC	10
■	GUAGCUAAUGACUAGCAUA	10
■	GUAGCAUGACUGUGACACGU *	10
■	GACAUCAAUGGGACAGCACC	10
■	UCCACGCAUCAAAGCAUGUC	10
■	UCCGCGACAAUCUACAGUGG *	10
■	UUUGAAAUUUAUGACGUGCA	10
■	ACGGUGAAAAGAUUUUAACCC	10
■	GUGUAUCGAUGUGCUACCUA	10
■	CAAACGGUAUCACCCAACUA	10
■	AGCAUCACGCCGUAUCGCAA	10
■	CGCUACCUACUGUCCGUCG	10

Table II. List of sequences and simulation duration. For 5 of 20 sequences we performed two independent runs: one of 10 ns and another of 100 ns. For the remaining 15 sequences only 10 ns were performed. The color in the first column is that used in the labels of Fig. 11. The three sequences labeled with a "*" show very strong deviations from the average behavior of the q -stiffnesses of Fig. 11. These deviations involve in particular \tilde{A}'_q and \tilde{C}_q . An analysis of these two sequences show that these have a strong multimodal behavior. A comparison of the q -stiffnesses for the 10 ns and 100 ns simulations for the top 5 sequences are shown in Fig. 12.

Appendix A: Details of all-atom simulations

Twenty all-atom simulations were performed of different oligonucleotides of dsRNA, the sequences are listed in Table II along with the simulation time. The all-atom simulations were performed using Gromacs³⁸ (version 2018.4). The atomic structure of the dsRNA sequences in Table II were obtained with the x3DNA webtool³⁹. This structure was put in the center of a dodecahedral simulation box leaving 2 nm of free space on either side of the dsRNA molecule. Periodic boundary conditions were defined over the simulation box and the simulation domain was filled with water and 150 mM NaCl. Additional Na⁺ was added as to produce a charge neutral system. We used the TIP3P water model⁴⁰. Before starting the simulation run the energy of the system was minimized such that the maximum force throughout the system does not exceed the threshold of 1000 kJ mol⁻¹ nm⁻¹. Interactions were derived from the OL15 nucleic acid package⁴¹ which is based on the amber ff99 + bsc0 force field and contains the χ_{OL3} dihedral improvement for RNA⁴². This force field was chosen for its easy availability and because it is a well tested standard choice^{43,44}. Regarding force fields for all-atom simulations of RNA it should be noted that progress has been made during past years⁴⁵. However, considering the purpose of our simulations was to demonstrate the presence of length-scale-dependent elasticity and non-local couplings rather than precise measurement of local parameters, the es-

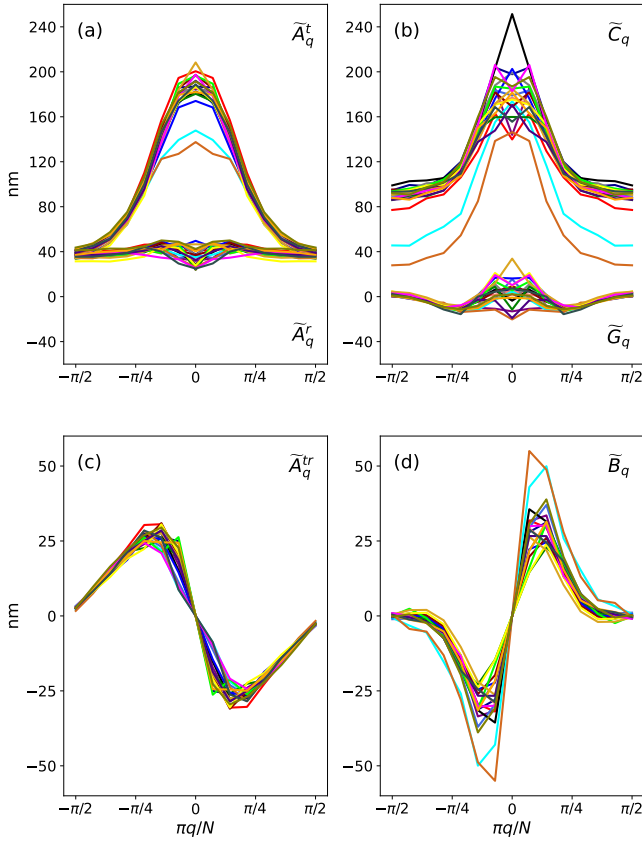


Figure 11. Momentum-space stiffnesses as obtained for each individual oligonucleotide. The color of the plots refer to their corresponding sequence as indicated in Table II. The data displayed for dsRNA in Figure 2 is obtained by averaging over all oligomers.

established Amber ff99bsc0 χ_{OL3} suffices.

Non-bonded interactions were cut-off at 1 nm and long range electrostatic interactions were handled through the particle-mesh Ewald algorithm. After energy minimisation, the system was equilibrated to a temperature of 300 K through a molecular dynamics run of 100 ps. The constant temperature was enforced by using the velocity-rescaling thermostat⁴⁶. Subsequently the system was equilibrated for 100 ps to a pressure of 1 bar where the pressure was enforced with a Parrinello-Rahman barostat⁴⁷. After equilibration, molecular dynamics simulations of 10 or 100 ns were performed at 300 K. The dsRNA configurations were stored every 1 ps. The DNA data shown in Fig. 2, were taken from Ref. 13 where they were generated using a very similar procedure using the parmbsc1 force field⁴⁸, which is specific to DNA.

The ensemble of snapshots obtained in this way, were analysed using the Curves+ software¹⁹ in order to obtain an equilibrium sampling of deformation parameters Δ_n and their Fourier transforms from (3). The momentum-space stiffness coefficients for various oligonucleotides are shown in Fig. 11 (for simulation times of 10 ns). Figure 12 shows a comparison between the 10 ns (solid lines) and the 100 ns (dashed lines) simulation runs for the first five sequences of Table II. In four of these sequences we find good overlap between the

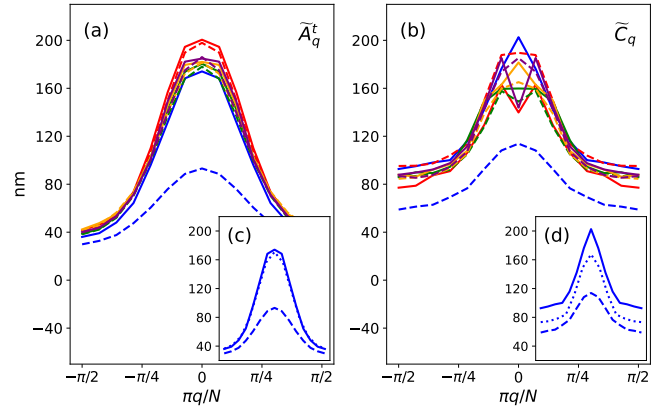


Figure 12. Comparison of the momentum-space (a) tilt and (b) twist stiffnesses obtained from 10 ns (solid) and 100 ns (dashed) all-atom simulation for five sequences of dsRNA. The sequences are the top five of Table II (same color code is used). Whilst good correspondence between the momentum space elasticity coefficients obtained from 10 ns and 100 ns simulations is found for four of the five simulated sequences, substantial deviations for \tilde{A}_q^t and \tilde{C}_q are found for the AAAACGAGGAUCUUAUCUCG sequence (blue). After inspection, the inconsistency was ascribed to a bimodality found in the AAAAC step. The insets (c) and (d) show the details of the stiffnesses for this sequence, showing the 10 ns simulation data (solid) the 100 ns simulation data (dashed) and the 100 ns simulation data with A-tract removed (dotted).

long and short simulation runs. One sequence (blue lines), corresponding to the first entry in Table (II) shows a rather different behavior for the short and long runs, due to the bimodal distribution associated to the A-tracts (see caption of Fig. 12 for discussion). Bimodality⁴⁹ here means a breakdown of the harmonic model, which assumes gaussian fluctuations of the variables around their equilibrium point. For long simulation runs tilt and twist show a bimodal distribution fluctuating between two distinct values, which gives a large variance and as a consequence low stiffness. During analysis, the two terminal base-pairs steps at both sides were omitted to avoid fraying effects.

Appendix B: Real space couplings

From the stiffnesses in momentum space, the real space stiffness can be deduced by taking the inverse Fourier transform. Since the real-space couplings between distant sites decays rapidly with increasing distance, the off-site couplings can be retrieved by fitting the data with functions of the form:

$$\tilde{X}_q^{even} = \sum_m X_m \cos \frac{2\pi m q}{N} \quad (\text{B1})$$

And

$$\tilde{X}_q^{odd} = \sum_m X_m \sin \frac{2\pi m q}{N} \quad (\text{B2})$$

Where X_m is an element of real-space stiffness matrix M_m and \tilde{X}_q the corresponding element in \tilde{M}_q . The fits are for even and

N=15	X_0	X_1	X_2	X_3	X_4	X_5
A_q^l	94	67	13	1.0	-1.1	-0.5
A_q^r	38	0.9	-1.9	-1.5	-0.6	-0.2
\tilde{C}_q	112	41	15	2.4	-2.1	-2.2
A_q^{lr}	0	-23	-4.4	-1.1	0.3	-0.3
\tilde{B}_q	0	16	14	5.7	1.5	0.3
\tilde{G}_q	-4.3	0.3	6.8	1.1	-0.6	-0.4
$C_q^{(h)}$	67	18	9.2	1.5	-0.7	-0.4

Table III. Real space stiffnesses X_m for dsRNA as obtained from fits of the corresponding momentum space stiffnesses \tilde{X}_q displayed in Figure 2.

odd functions of q respectively. The resulting real-space stiffnesses from this fitting procedure are shown in Table III. The resulting values of A_m^l and C_m substantiate the non-locality of tilt and twist deformations having significant beyond nearest-neighbour couplings, in contrast the range of roll-roll interactions is limited. The results illustrate that non-local couplings are not unique to DNA, but are also found in other double-helical biomolecules.

Appendix C: Twist stiffness in the ladder model

We derive here Eqs. (27) and (28) giving the twist stiffness of the modes $q = 0$ and $q = q_{\max}$ shown in Fig. 8(c) and (d). Let us consider first the mode $q = 0$. The positions of the masses on the two strands are in this case given by:

$$\vec{a}_n^\pm = \frac{l_0}{2} \left[\pm \cos(n\omega), \pm \sin(n\omega), 2n \cos \frac{\omega}{2} \right] \quad (C1)$$

These describe two helices winding around the z axis and with constant twist angle ω . The diameter of the helices is l_0 and the pitch $\frac{2\pi l_0}{\omega} \cos(\omega/2)$. The bond vectors (defined as in Fig. 5) for the two strands are:

$$\vec{u}_n = \vec{a}_{n+1}^+ - \vec{a}_n^+, \quad \vec{v}_n = \vec{a}_{n+1}^- - \vec{a}_n^-, \quad (C2)$$

while the rungs of the ladder are

$$\vec{x}_n = \vec{a}_n^+ - \vec{a}_n^- \quad (C3)$$

The definition (C1) implies that $|\vec{u}_n| = |\vec{v}_n| = |\vec{x}_n| = l_0$. The stacking contribution to the energy is obtained from

$$\frac{\vec{x}_n \cdot \vec{x}_{n+1}}{l_0^2} = \cos \omega \approx 1 - \frac{\omega^2}{2} \quad (C4)$$

while to estimate the backbone bending contribution we need to compute

$$\frac{\vec{u}_{n+1} \cdot \vec{u}_n}{l_0^2} = 1 - (1 - \cos \omega) \sin^2 \left(\frac{\omega}{2} \right) \approx 1 - \frac{\omega^4}{8} \quad (C5)$$

For the angles we have

$$\sin \theta_{n,1} = \sqrt{1 - \left(\frac{\vec{x}_n \cdot \vec{u}_n}{l_0^2} \right)^2} \approx 1 - \frac{\omega^4}{32} \quad (C6)$$

and similar relations for $\theta_{n,2}$, $\theta_{n,3}$ and $\theta_{n,4}$. Equations (C5) and (C6) imply that the energy of the $q = 0$ twist mode is independent on K_{wlc} and K_a , as these couple to higher order anharmonic terms ($\sim \omega^4$). The only contribution to order ω^2 comes from the stacking (C4), which leads to Eq. (27).

The positions of the masses in the mode $q = q_{\max}$ are

$$\vec{a}_n^\pm = \frac{l_0}{2} \left[\pm \cos \frac{\omega}{2}, \pm \sin \frac{(-1)^n \omega}{2}, 2n \cos \frac{\omega}{2} \right] \quad (C7)$$

In this case a step from site n (even) to site $n+1$ (odd) corresponds to a twist deformation with twist angle $-\omega$, while a step from an odd to an even site corresponds to a twist angle $+\omega$. The calculation of the stacking term is as above and leads to (C4). The bending of the backbone is different from the $q = 0$ case and it is given by

$$\frac{\vec{u}_{n+1} \cdot \vec{u}_n}{l_0^2} = \cos \omega \approx 1 - \frac{\omega^2}{2} \quad (C8)$$

We find for the angles

$$\frac{\vec{x}_n \cdot \vec{u}_n}{l_0^2} = -\sin^2 \left(\frac{\omega}{2} \right) \approx -\frac{\omega^2}{4} \quad (C9)$$

which as is the case of (C6) gives rise to a higher order anharmonic term $\sim \omega^4$ for all angular interactions. Summarizing, the harmonic contributions to the q_{\max} mode are stacking (C4) and bending (C8). Combining these two one gets Eq. (28).

In a similar fashion the calculation for the twist stiffness \tilde{C}_q can be extended to entail an arbitrary q -mode. For the ladder model with local stacking interactions such a calculation yields:

$$\tilde{C}_q = K_{wlc} \left(1 - \cos \frac{2\pi q}{N} \right) + K_{st} \quad (C10)$$

Which interpolates between the estimates of Eq. (27) and (28). The estimate of Eq. (C10) is compared with the results from Monte Carlo simulations in Figure 7(c). For a ladder with non-local stacking interactions, one obtains:

$$\tilde{C}_q = K_{wlc} \left(1 - \cos \frac{2\pi q}{N} \right) + K_{st} + \sum_{l>1} K_{st}^{(l)} \left(l + 2 \sum_{j=1}^{l-1} (l-j) \cos \left(\frac{2\pi j q}{N} \right) \right) \quad (C11)$$

Where the summation in l runs over all non-local stacking interactions $K_{st}^{(l)}$. For $q = 0$ and $q = q_{\max}$ Eq. (C11) reduces to (31) and (32), correspondingly. In Fig. 9(c) the derived q -dependence of the twist stiffness (C11) is compared to the twist q -stiffness obtained from simulations.

REFERENCES

- ¹A. Aggarwal, S. Naskar, A. K. Sahoo, S. Mogurampelly, A. Garai, and P. K. Maiti, "What do we know about DNA mechanics so far?" *Curr. Op. Struct. Biol.* **64**, 42 – 50 (2020).

- ²H. Dohnalová and F. Lankaš, “Deciphering the mechanical properties of B-DNA duplex,” *WIREs Comput Mol Sci.*, e1575 (2021).
- ³A. Marin-Gonzalez, J. Vilhena, R. Perez, and F. Moreno-Herrero, “A molecular view of DNA flexibility,” *Quarterly Reviews of Biophysics* **54**, e8 (2021).
- ⁴F. Lankaš, J. Šponer, J. Langowski, and T. E. Cheatham, “DNA basepair step deformability inferred from molecular dynamics simulations,” *Biophys J.* **85**, 2872–2883 (2003).
- ⁵A. Noy and R. Golestanian, “Length scale dependence of DNA mechanical properties,” *Phys. Rev. Lett.* **109**, 228101 (2012).
- ⁶M. Pasi, J. H. Maddocks, D. Beveridge, T. C. Bishop, D. A. Case, T. Cheatham, P. D. Dans, B. Jayaram, F. Lankas, C. Laughton, J. Mitchell, R. Osman, M. Orozco, A. Pérez, D. Petkeviciute, N. Spackova, J. Sponer, K. Zakrzewska, and R. Lavery, “ μ ABC: A systematic microsecond molecular dynamics study of tetranucleotide sequence effects in B-DNA,” *Nucl. Acids Res.* **42**, 12272–12283 (2014).
- ⁷V. Velasco-Berrelleza, M. Burman, J. W. Shepherd, M. C. Leake, R. Golestanian, and A. Noy, “SerraNA: a program to determine nucleic acids elasticity from simulation data,” *Phys. Chem. Chem. Phys.* **22**, 19254 (2020).
- ⁸J. Walther, P. D. Dans, A. Balaceanu, A. Hospital, G. Bayarri, and M. Orozco, “A multi-modal coarse grained model of DNA flexibility mappable to the atomistic level,” *Nucl. Acids Res.* **48**, e29–e29 (2020).
- ⁹P. D. Dans, A. Zeida, M. R. Machado, and S. Pantano, “A coarse grained model for atomic-detailed DNA simulations with explicit electrostatics,” *J. Chem. Theory Comput.* **6**, 1711–1725 (2010).
- ¹⁰P. Šulc, F. Romano, T. E. Ouldridge, L. Rovigatti, J. P. K. Doye, and A. A. Louis, “Sequence-dependent thermodynamics of a coarse-grained DNA model,” *J. Chem. Phys.* **137**, 135101 (2012).
- ¹¹E. Skoruppa, M. Laleman, S. Nomidis, and E. Carlon, “DNA elasticity from coarse-grained simulations: The effect of groove asymmetry,” *J. Chem. Phys.* **146**, 214902 (2017).
- ¹²D. Chakraborty, N. Hori, and D. Thirumalai, “Sequence-dependent three interaction site model for single- and double-stranded DNA,” *J. Chem. Theory Comput.* **14**, 3763–3779 (2018).
- ¹³E. Skoruppa, A. Voorspoels, J. Vreede, and E. Carlon, “Length-scale-dependent elasticity in DNA from coarse-grained and all-atom models,” *Phys. Rev. E* **103**, 042408 (2021).
- ¹⁴M. Segers, E. Skoruppa, J. A. Stevens, M. Vangilbergen, A. Voorspoels, and E. Carlon, “Comment on ‘Flexibility of short DNA helices with finite-length effect: From base pairs to tens of base pairs’,” *J. Chem. Phys.* **155**, 027101 (2021).
- ¹⁵F. Lankaš, O. Gonzalez, L. Heffler, G. Stoll, M. Moakher, and J. H. Maddocks, “On the parameterization of rigid base and basepair models of DNA from molecular dynamics simulations,” *Phys. Chem. Chem. Phys.* **11**, 10565–10588 (2009).
- ¹⁶B. Eslami-Mossallam and M. Ejtehadi, “Contribution of nonlocal interactions to DNA elasticity,” *J. Chem. Phys.* **134**, 03B623 (2011).
- ¹⁷R. Lavery, K. Zakrzewska, D. Beveridge, T. C. Bishop, D. A. Case, T. Cheatham, S. Dixit, B. Jayaram, F. Lankas, C. Laughton, J. H. Maddocks, A. Michon, R. Osman, M. Orozco, A. Perez, T. Singh, N. Spackova, and J. Sponer, “A systematic molecular dynamics study of nearest-neighbor effects on base pair and base pair step conformations and fluctuations in B-DNA,” *Nucl. Acids Res.* **38**, 299–313 (2010).
- ¹⁸O. Gonzalez, D. Petkeviciute, and J. Maddocks, “A sequence-dependent rigid-base model of DNA,” *J. Chem. Phys.* **138**, 02B604 (2013).
- ¹⁹R. Lavery, M. Moakher, J. Maddocks, D. Petkeviciute, and D. Zakrzewska, “Conformational analysis of nucleic acids revisited: Curves+,” *Nucl. Acids Res.* **37**, 5917–5929 (2009).
- ²⁰J. Marko and E. Siggia, “Bending and twisting elasticity of DNA,” *Macromolecules* **27**, 981–988 (1994).
- ²¹E. Skoruppa, S. Nomidis, J. F. Marko, and E. Carlon, “Bend-Induced Twist Waves and the Structure of Nucleosomal DNA,” *Phys. Rev. Lett.* **121**, 088101 (2018).
- ²²M. Caraglio, E. Skoruppa, and E. Carlon, “Overtwisting induces polygonal shapes in bent DNA,” *J. Chem. Phys.* **150**, 135101 (2019).
- ²³S. K. Nomidis, E. Skoruppa, E. Carlon, and J. F. Marko, “Twist-bend coupling and the statistical mechanics of the twistable wormlike-chain model of DNA: perturbation theory and beyond,” *Phys. Rev. E* **99**, 032414 (2019).
- ²⁴Y. A. G. Fosado, F. Landuzzi, and T. Sakaue, “Twist dynamics and buckling instability of ring DNA: the effect of groove asymmetry and anisotropic bending,” *Soft Matter* **17**, 1530–1537 (2021).
- ²⁵J. F. Marko and E. D. Siggia, “Stretching DNA,” *Macromolecules* **28**, 8759–8770 (1995).
- ²⁶J. Lipfert, G. M. Skinner, J. M. Keegstra, T. Hensgens, T. Jager, D. Dulin, M. Köber, Z. Yu, S. P. Donkers, F.-C. Chou, R. Das, and N. H. Dekker, “Double-stranded RNA under force and torque: Similarities to and striking differences from double-stranded DNA,” *Proc. Natl. Acad. Sci. USA* **111**, 15408–15413 (2014).
- ²⁷E. Herrero-Galán, M. E. Fuentes-Perez, C. Carrasco, J. M. Valpuesta, J. L. Carrascosa, F. Moreno-Herrero, and J. R. Arias-Gonzalez, “Mechanical identities of RNA and DNA double helices unveiled at the single-molecule level,” *J. Am. Chem. Soc.* **135**, 122–131 (2013).
- ²⁸A. Marin-Gonzalez, J. Vilhena, R. Perez, and F. Moreno-Herrero, “Understanding the mechanical response of double-stranded DNA and RNA under constant stretching forces using all-atom molecular dynamics,” *Proc. Natl. Acad. Sci.* **114**, 7049–7054 (2017).
- ²⁹J. Abels, F. Moreno-Herrero, T. van der Heijden, C. Dekker, and N. Dekker, “Single-molecule measurements of the persistence length of double-stranded RNA,” *Biophys. J.* **88**, 2737–2744 (2005).
- ³⁰Y.-T. Chen, H. Yang, and J.-W. Chu, “Structure-mechanics statistical learning unravels the linkage between local rigidity and global flexibility in nucleic acids,” *Chemical science (Cambridge)* **11**, 4969–4979 (2020).
- ³¹M. Segers, *Length scale dependent elasticity in Nucleic Acids* (Master Thesis, KU Leuven, 2021).
- ³²R. Everaers, R. Bundschuh, and K. Kremer, “Fluctuations and stiffness of double-stranded polymers: railway-track model,” *EPL (Europhys. Lett.)* **29**, 263 (1995).
- ³³C. Heussinger, M. Bathe, and E. Frey, “Statistical mechanics of semiflexible bundles of wormlike polymer chains,” *Phys. Rev. Lett.* **99**, 048101 (2007).
- ³⁴B. S. Fujimoto and J. M. Schurr, “Dependence of the torsional rigidity of DNA on base composition,” *Nature* **344**, 175–178 (1990).
- ³⁵S. K. Nomidis, F. Kriegel, W. Vanderlinden, J. Lipfert, and E. Carlon, “Twist-Bend Coupling and the Torsional Response of Double-Stranded DNA,” *Phys. Rev. Lett.* **118**, 217801 (2017).
- ³⁶P. D. Dans, J. Walther, H. Gomez, and M. Orozco, “Multiscale simulation of DNA,” *Curr. Op. Struct. Biol.* **37**, 29–45 (2016).
- ³⁷S. Sankararaman and J. F. Marko, “Formation of loops in DNA under tension,” *Phys. Rev. E* **71**, 021911 (2005).
- ³⁸M. Abrahams, T. Murtola, R. Schulz, S. Páll, J. Smith, B. Hess, and E. Lindahl, “GROMACS: high performance molecular simulations through multi-level parallelism from laptops to supercomputers,” *SoftwareX* **1-2**, 19–25 (2015).
- ³⁹S. Li, W. Olson, and X.-J. Lu, “Web 3dna - a web server for the analysis, visualisation, and modelling of 3d nucleic acid structures,” *Nucl. Acids Res.* **47**, W26–W34 (2019).
- ⁴⁰W. L. Jorgensen, J. Chandrasekhar, J. D. Madura, R. W. Impey, and M. L. Klein, “Comparison of simple potential functions for simulating liquid water,” *J. Chem. Phys.* **79**, 926–935 (1983).
- ⁴¹M. Zgarbova, J. Sponer, M. Otyepka, T. E. Cheatham, R. Galindo-Murillo, and P. Jurecka, “Refinement of the sugar-phosphate backbone torsion beta for AMBER force fields improves the description of Z- and B-DNA,” *J. Chem. Theory Comput.* **11**, 5723–5736 (2015).
- ⁴²M. Zgarbova, M. Otyepka, J. Sponer, A. Mladek, P. Banas, T. E. Cheatham, and P. Jurecka, “Refinement of the Cornell et al. Nucleic Acids Force Field Based on Reference Quantum Chemical Calculations of Glycosidic Torsion Profiles,” *J. Chem. Theory Comput.* **7**, 2886–2902 (2011).
- ⁴³P. D. Dans, I. Ivani, A. Hospital, G. Portella, C. Gonzalez, and M. Orozco, “How accurate are accurate force-fields for B-DNA?” *Nucl. Acids Res.* **45**, 4217–4230 (2017).
- ⁴⁴J. Sponer, G. Bussi, M. Krepl, P. Banas, S. Bottaro, R. A. Cunha, A. Gil-Ley, G. Pinamonti, S. Pobleto, P. Jurecka, *et al.*, “RNA structural dynamics as captured by molecular simulations: a comprehensive overview,” *Chem. Rev.* **118**, 4177–4338 (2018).
- ⁴⁵D. Tan, S. Piana, R. M. Dirks, and D. E. Shaw, “RNA force field with accuracy comparable to state-of-the-art protein force fields,” *PNAS* **115**, E1346–E1355 (2018).
- ⁴⁶G. Bussi, D. Donadio, and M. Parrinello, “Canonical sampling through velocity rescaling,” *J. Chem. Phys.* **126** (2007), 10.1063/1.2408420.

- ⁴⁷M. Parrinello and A. Rahman, "Polymorphic transitions in single crystals: A new molecular dynamics method," *J. Appl. Phys.* **52**, 7182–7190 (1981).
- ⁴⁸I. Ivani, P. Dans, A. Noy, A. Pérez, I. Faustino, A. Hospital, J. Walther, P. Andrio, R. Goñi, A. Balaceanu, G. Portella, F. Battistini, J. Gelpí, C. González, M. Vendruscolo, C. Lughton, S. Harris, D. Case, and M. Orozco, "Parmbsc1: a refined force field for DNA simulations," *Nat. Methods* **13**, 55–58 (2016).
- ⁴⁹P. D. Dans, A. Perez, I. Faustino, R. Lavery, and M. Orozco, "Exploring polymorphisms in B-DNA helical conformations," *Nucl. Acids Res.* **40**, 10668–10678 (2012).